

The radial velocity curve for He II emission cannot be used for component mass determination in SS433

A.V. DODIN ,¹ K.A. POSTNOV ,¹ AND A.M. CHEREPASHCHUK ,¹

¹*Sternberg Astronomical Institute, Lomonosov Moscow State University, Universitetskij prospekt 13, 119234 Moscow, Russia*

ABSTRACT

More than 150 measurements of the He II 4686 Å emission line in spectra of SS433 were obtained during 388 nights in 2020 – 2025 with the Transient Double-beam Spectrograph on the 2.5 m telescope of Caucasian Mountain Observatory of Sternberg Astronomical Institute. We found that the He II emission line formation region is not eclipsed and is significantly larger than both the donor star and the photosphere of the supercritical accretion disk. The He II radial velocity curve was found to be independent of the precessional phase and inconsistent with the photometric curve. These findings suggest that the He II line does not reflect the orbital motion of the compact object. Therefore, spectroscopic estimates of the masses of the components in SS433 based on the He II emission line can be unrealistic.

Keywords: Stellar accretion disks (1579) — HMXB (777) — Stellar mass black holes (1611)

1. INTRODUCTION

The Galactic microquasar SS433 is a massive eclipsing X-ray binary system at an advanced evolutionary stage with a supercritical accretion disk around a black hole and relativistic jets (B. Margon 1984; S. Fabrika 2004; A. Cherepashchuk et al. 2020; A. M. Cherepashchuk et al. 2025). The object displays three variabilities: orbital ($P_{\text{orb}} \approx 13^d.1$), precessional ($P_{\text{prec}} \approx 162^d.3$), and nutational ($P_{\text{nut}} = 6^d.29$) ones. Spectroscopic studies of SS433 as a close binary system have been carried out by many authors. From Doppler shifts of narrow components of stationary hydrogen emission lines, a period of $13^d.1$ was detected, suggesting that SS433 is a close binary system (D. Crampton et al. 1980). In the paper by A. M. Cherepashchuk (1981), optical eclipses were discovered in the SS433 system and it was shown that radial velocity curves constructed from stationary hydrogen emission lines (D. Crampton et al. 1980) do not reflect the orbital motion of the components since their shape is inconsistent with the positions of the primary and secondary minima on the light curve.

The discovery of double-peaked profiles of stationary hydrogen and neutral helium emission lines suggested the existence of a circumbinary shell around SS433 rotating with a velocity of about 200 km s^{-1} (A. V. Fil-

ippenko et al. 1988; M. G. Bowler 2011). The presence of a circumbinary disk with this rotation velocity was confirmed by interferometric measurements in the Br γ line at a distance of ~ 5 au from the central source (I. Waisberg et al. 2019), which implies a very high total mass of SS433 ($\gtrsim 400 M_{\odot}$) assuming the Keplerian rotation. Other observations presented in the same paper, but performed at a different time, show that the line profiles are dominated by a bipolar outflow. Despite such a complex and variable formation region of hydrogen lines, their average radial velocity reflects the orbital periodicity of the binary system, but does not provide information about the radial velocities of the components. Actually, the fact that the maximum of the radial velocity occurs in the middle of the eclipse reflects the flux-averaged motion of different emitting regions, including the powerful gas flow feeding the accretion disk or matter escaping through the outer Lagrangian point (W. Lu et al. 2023).

Starting from paper (D. Crampton & J. B. Hutchings 1981), the radial velocity curve of a compact object has been determined using the He II 4686 Å emission line. The semiamplitude of this radial velocity curve was found to be $\sim 195 \text{ km s}^{-1}$ corresponding to the mass function of the compact component:

$$f_X(m) = \frac{m_V^3 \sin^3 i}{(m_X + m_V)^2} \approx 10.1 M_{\odot}. \quad (1)$$

Here, m_V and m_X are the masses of the optical star and the compact object, respectively, and $i \approx 79^\circ$ is the binary inclination angle estimated from the moving emission lines. Observations carried out by [S. N. Fabrika & L. V. Bychkova \(1990\)](#) confirmed the result of [D. Crampton & J. B. Hutchings \(1981\)](#) and reported the mass function of SS433 $f_X(m) \approx 8M_\odot$ based on the He II 4686 Å emission. On the other hand, from measurements of the He II 4686 Å emission line, [S. D'Odorico et al. \(1991\)](#) obtained a significantly lower semiamplitude of the radial velocity curve $K_X \simeq 112 \text{ km s}^{-1}$, corresponding to $f_X(m) \approx 2M_\odot$.

Conclusions about the nature of the compact object in SS433 made by different authors based on high-quality spectroscopic observations are contradictory. For example, [S. D'Odorico et al. \(1991\)](#) claimed that the relativistic object in SS433 is a neutron star. The results of [K. Kubota et al. \(2010\)](#) also do not exclude a neutron star in SS433. According to [T. C. Hillwig et al. \(2004\)](#) and [P. Picchi et al. \(2020\)](#), the compact object in SS433 can be a relatively low-mass black hole $\sim 4M_\odot$. Recently, in the SS433 system, a secular increase in the orbital period was discovered at a rate of $(1.14 \pm 0.25) \times 10^{-7} \text{ ss}^{-1}$ ([A. M. Cherepashchuk et al. 2021](#)). The orbital angular momentum balance taking into account wind outflow from the supercritical accretion disk in SS433 implies that the mass ratio of the components should be $q = m_X/m_V > 0.8$, and the mass of the compact object is $m_X > 8M_\odot$. Moreover, the presence of a neutron star with mass $< 2.5M_\odot$ in SS433 is rejected because, in that case, the orbital period of the system should decrease, which contradicts observations ([A. Cherepashchuk et al. 2023](#)). Throughout the paper, we use the newest ephemeris ([A. Cherepashchuk et al. 2023](#)), which in 2020 – 2025 can be approximated with a constant period. Thus, the orbital phases of our observations are calculated as

$$\varphi_{\text{orb}} = (\text{HJD} - 2458933.136)/13.08341. \quad (2)$$

Historical data should be phased with actual values for the initial epoch and period. The precessional phases are calculated following [V. Goranskij \(2011\)](#):

$$\varphi_{\text{prec}} = (\text{HJD} - 2450003)/162.284. \quad (3)$$

The ambiguity in the inference about the mass of the compact object in SS433 from spectroscopic data may be due to the fact that a relatively short series of spectral observations was used. In this paper, we study the behavior of the He II line by carrying out an one order of magnitude longer series of homogeneous spectroscopic observations of SS433 than in the previous studies. This enables us to average random deviations in the position

and intensity of the line in order to construct the mean radial velocity curve from the He II emission at different phases of the 162 day precessional period.

2. OBSERVATIONS

We have performed spectral observations of SS433 during 388 nights in 2020 – 2025 using the 2.5 m telescope of the Caucasian Mountain Observatory of Sternberg Astronomical Institute of Moscow State University (CMO SAI MSU) with a low-resolution Transient Double-beam Spectrograph (TDS) ([S. A. Potanin et al. 2020](#)). The observations were carried out with a slit of 1'', which provides a spectral resolving power near the He II line of about $\lambda/\text{FWHM} \approx 1000$ and an accuracy of radial velocity measurements of $\sim 20 \text{ km s}^{-1}$. Each observation consisted of three frames with 300 s exposure, which resulted in a signal-to-noise ratio of about 30 at 4500 Å. In addition to our spectral data, we have used photometric BVRcIc observations of SS433 performed on the 60 cm RC600 telescope of CMO SAI MSU ([L. N. Berdnikov et al. 2020](#)).

3. RESULTS

Higher-resolution spectrographs than TDS revealed the double-peak structure of the He II 4686 Å line profile ([S. D'Odorico et al. 1991; P. Picchi et al. 2020](#)). With the lower TDS resolution, these peaks usually merge, but at certain moments the line profile widens and splits with a separation between the peaks of up to 2500 km s^{-1} (see Figure 1 and Figure 2). A similar broadening is observed on the same dates in the hydrogen and neutral helium lines. For radial velocity measurements, we selected only those dates where no moving line is superimposed on the stationary He II emission and where the profile's middle can be uniquely determined by fitting a single Gaussian. Most of these cases occur at the precessional phases near the maximum disk opening to the viewer (moment T3, $\varphi_{\text{prec}} = 0$); however, profiles with regular shape can occur in other phases, too. Examples of the profiles used for the radial velocity measurements are shown in Figure 3.

In Figure 4a, we plot 92 measurements at phases $-0.2 < \varphi_{\text{prec}} < 0.2$ and 66 at the remaining phases. The radial velocity curve demonstrates a random spread apparently related to the multicomponent and variable structure of the line profile that is not resolved by the TDS spectrograph. The magnitude of these variations depends on the precessional phase and is minimal at phases around $\varphi_{\text{prec}} = 0$ and $\varphi_{\text{prec}} = 0.5$. The average radial velocity curve does not exhibit statistically significant changes at different precessional phases, which were noted in previous works (see, for example, [S. N.](#)

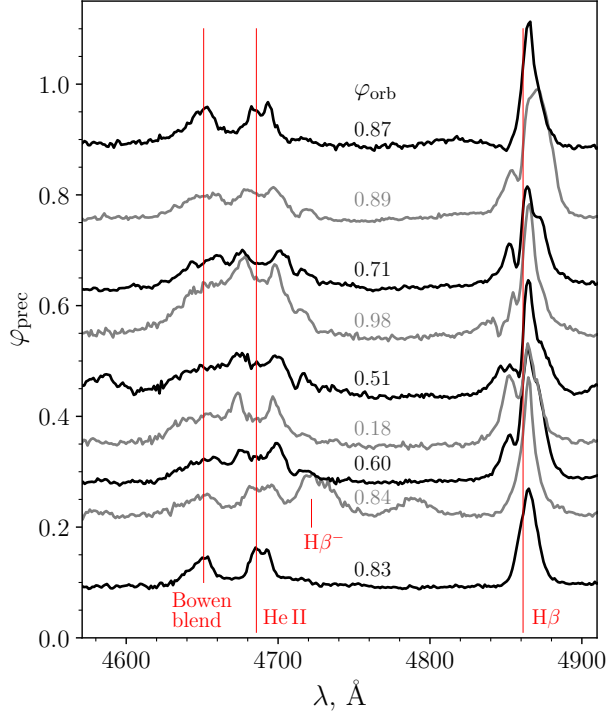


Figure 1. Examples of TDS spectra of SS433 at dates with double-peaked He II 4686 Å line.

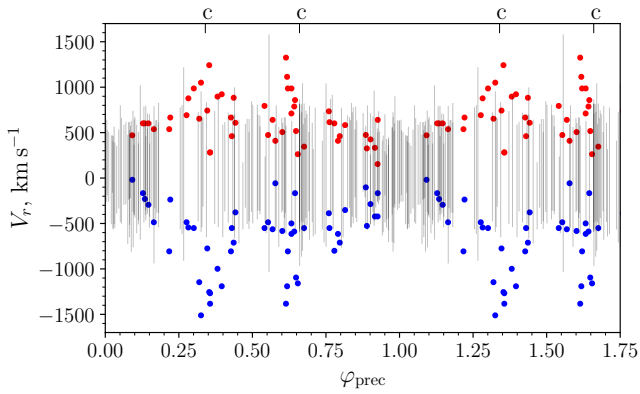


Figure 2. The appearance of double-peaked profiles as a function of the precessional phase. Red and blue dots mark the velocities of each peak. Gray lines mark the position and FWHM of all single-peaked profiles used for constructing the radial velocity curve shown in Figure 4. Crossover phases (disk edge-on) are marked with “c” labels at the top.

Fabrika & L. V. Bychkova 1990). Only a slight increase in the probability of appearance of wide double-peaked profiles can be suspected at the crossover precessional phases when the disk is visible edge-on (see Figure 2). However, we stress that there is no regular dependence of deviations of the He II radial velocity from the mean value on the precessional phase (see Figure 5).

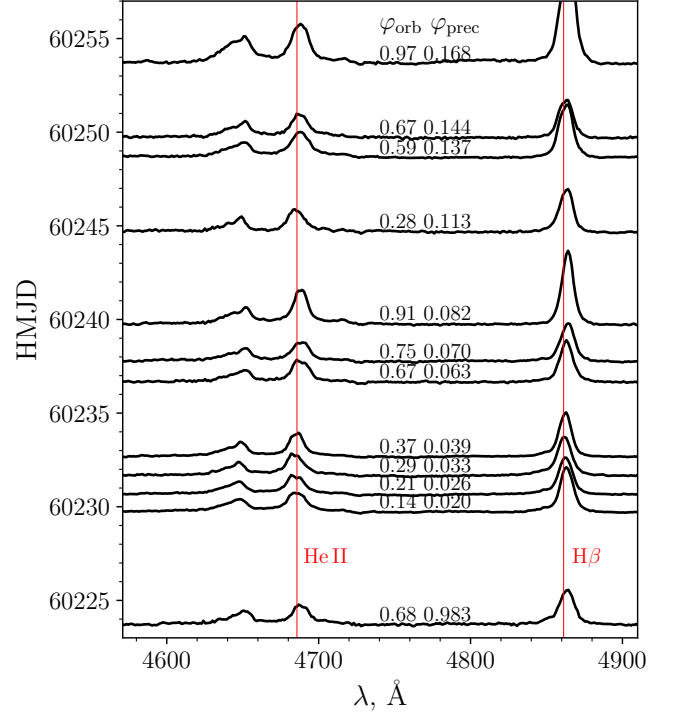


Figure 3. Examples of TDS spectra of SS433 used for measurements of radial velocities of He II.

4. DISCUSSION

It can be assumed that the discrepancies in the parameters of the radial velocity curve SS433 obtained by various authors are associated with a small number of spectra used in the presence of natural velocity fluctuations due to distortions of the He II line profile. For comparison, we have superimposed our radial velocity curve with measurements from K. Kubota et al. (2010), as well as our with own measurements from archive X-shooter² spectra of SS433 (J. Vernet et al. 2011), which are described in P. Picchi et al. (2020). These data are consistent with our measurements within a random dispersion.

4.1. Peculiarity of the radial velocity curve from He II emission

The number of points in the radial velocity curve obtained is already sufficient to see that it does not have a sinelike form, as was assumed in all previous studies. The differences from the sinelike form might be related to the SS433 orbital eccentricity $e = 0.05$, which we measured in A. M. Cherepashchuk et al. (2021) using the eclipsing light curve. However, by taking the orbital parameters from A. M. Cherepashchuk et al.

² <https://archive.eso.org/scienceportal>

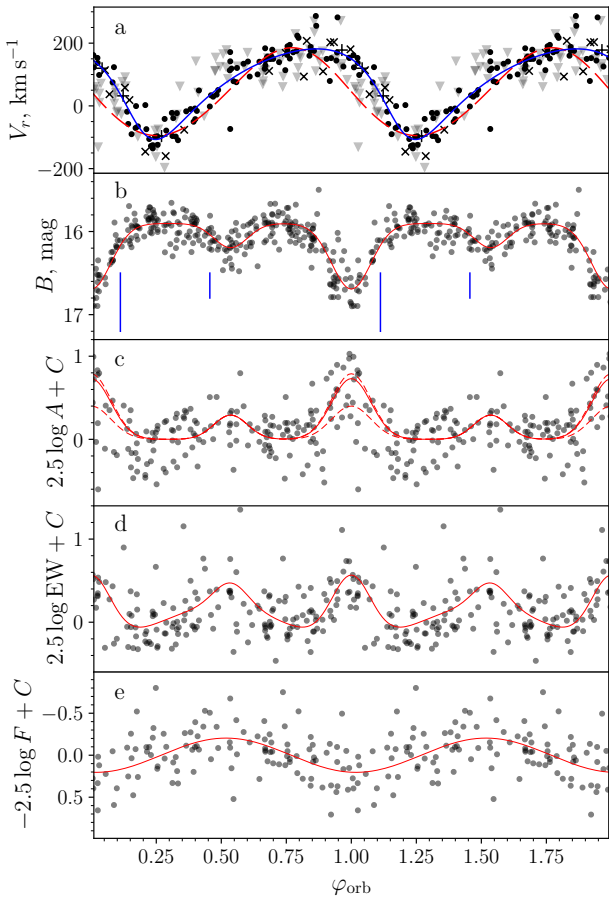


Figure 4. Orbital phase curves of He II 4686 Å line variability. (a) The radial velocity curve: black circles show our TDS observations at phases $-0.2 < \varphi_{\text{prec}} < 0.2$; gray triangles show our TDS observations at phases $0.2 < \varphi_{\text{prec}} < 0.8$; crosses “x” are our measurements from the X-shooter spectra, plus signs “+” are measurements from K. Kubota et al. (2010), the blue line is a formal fit to the radial velocities ($e = 0.30$, $K_X = 144 \text{ km s}^{-1}$, $\omega = 142^\circ$, $\gamma = 71 \text{ km s}^{-1}$); the red dashed curve corresponds to the radial velocities for the orbital parameters from A. M. Cherepashchuk et al. (2021) ($e = 0.05$, $\omega = 40^\circ$) scaled and shifted with $K_X = 140 \text{ km s}^{-1}$ and $\gamma = 40 \text{ km s}^{-1}$; (b) The photometric B light curve at phases $-0.2 < \varphi_{\text{prec}} < 0.2$, the red curve is the Gaussian fits of the primary and secondary minima. Blue vertical lines indicate the would-be positions of the primary and secondary minima for the formal fit to the He II radial velocity curve shown in blue in panel (a). (c) The He II 4686 Å line height relative to the continuum expressed in stellar magnitudes for ease of comparison with the light curve. The red solid curve is the “upside-down” red light curve shown in panel (b), scaled to best match with the observed change in the line height, which corresponds to the 6% eclipsed fraction of the He II line region. The upper dashed curve shows the expected change in the line height in the absence of an eclipse. The lower dashed curve corresponds to the 30% eclipsed fraction of the He II line flux. (d) The same as in panel (c) for the line equivalent width; the solid curve corresponds to no line eclipse, but takes into account a sinelike flux variability shown in panel (e). (e) Orbital variability of the He II line flux with a sinelike fit (red curve).

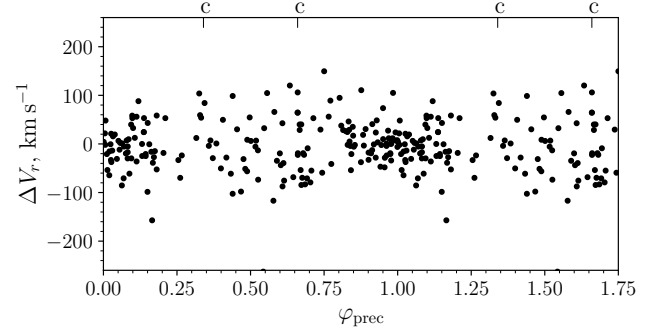


Figure 5. Deviations of the radial velocity of He II line from the formal fit in Figure 4a as a function of the precessional phase. No regular phase dependence is seen. Crossover phases are marked with “c” labels at the top.

(2021) we get an obvious difference between the observations and the expected radial velocity curve for any amplitude K_X and γ -velocity (see red dashed curve in Figure 4a for $K_X = 140 \text{ km s}^{-1}$ and $\gamma = 40 \text{ km s}^{-1}$). The formal solution of the observed radial velocity curve shown by the solid line in Figure 4a yields a much higher eccentricity $e = 0.30 \pm 0.03$ ($K_X = 144 \pm 4 \text{ km s}^{-1}$, $\omega = 142^\circ \pm 6^\circ$, $\gamma = 71 \pm 3 \text{ km s}^{-1}$, the periastron phase at $\varphi_{\text{orb}} = 0.191 \pm 0.015$, and $f_X(m) \approx 3.6 M_\odot$). However, the primary and secondary minima in the corresponding light curve for this radial velocity curve would occur at $\varphi_{\text{orb}} = 0.11 \pm 0.02$ and $\varphi_{\text{orb}} = 0.46 \pm 0.03$ instead of the observed $\varphi_{\text{orb}} = 0.0000 \pm 0.0008$ and $\varphi_{\text{orb}} = 0.5231 \pm 0.0012$ (see the blue marks in Figure 4b). Thus, if we interpret the obtained radial velocity curve as a consequence of the orbital motion of the line generation region, there would be a clear contradiction with the position of the minima on the light curve. As in the case of hydrogen lines (see the Introduction), this suggests that the radial velocity curve constructed from the He II line measurements does not reflect the true orbital motion of the compact object in SS433. For orbital parameters derived from the light curve of SS433, the discrepancy between the observed radial velocity curve from He II line measurements and the calculated radial velocity curve (red dashed line in Figure 4a) can be explained by additional factors, such as relative intensity change of the multicomponent line profile or additional emission (e.g., produced in matter flowing out from the external Lagrangian point and forming the circumbinary disk; see W. Lu et al. (2023)) also modulated by the orbital period. But such deviations would make the line unacceptable for the measurement of the compact object’s orbital motion.

4.2. Insignificant eclipse of the He II line formation region

It is usually assumed that the formation region of the He II 4686 Å line is associated with the accretion disk and/or the base of the relativistic jet. In this case, the line flux should exhibit eclipses at the phase $\varphi_{\text{orb}} = 0$ because with the orbital inclination $i = 79^\circ$ in SS433, the limb of the optical star should screen the accretion disk center at the mid-eclipse. [K. Kubota et al. \(2010\)](#) noted the profile variability near $\varphi_{\text{orb}} = 0$, which is attributed to the partial eclipse of the line formation region. However, our observations do not show systematic changes in the profile and/or the Rossiter-McLaughlin effect at phases $\varphi_{\text{orb}} \approx 0$.

To check whether the line formation region is eclipsed, we examined the change in the line height above the continuum in Figure 4c, as well as the equivalent width (EW) of the line in Figure 4d (the latter showed a greater dispersion due to the inaccuracy of the line width σ estimates when fitting it with a single Gaussian; however, it has a more clear physical meaning, so we present both curves). The dispersion of points on the plots is primarily related to the actual irregular change in the line flux, see, for example, Figure 3 from [P. Picchi et al. \(2020\)](#), where the line flux varies by a factor of two at the same precessional and orbital phases. From Figures 4cd it can be seen that the line's height and EW increase during both the primary and secondary eclipse minima in strict anticorrelation with the light curve. This is a reliable indication that the line formation region is not eclipsed substantially. The near-constant emission line flux appears stronger relative to the weakening continuum during eclipses, that is to say, such variability of the line height and EW reflects the contrast of the (quasi)constant emission line on top of the variable continuum.

For a quantitative description, we fitted the primary minimum on the light curve with a Gaussian, and then found the height of the Gaussian with the same position and width for the He II line height change. From the ratio of amplitudes of the Gaussians, we found that the optimal value of the eclipsed part of the line is $6\% \pm 7\%$ (solid line in Figure 4c) that is, the data can be consistent even with the complete absence of the eclipsed part (upper dashed line in Figure 4c). The largest fraction of the eclipsed line flux cannot exceed 30% (lower dashed line in Figure 4c). Thus, most of the He II 4686 Å line flux is produced far from the accretion disk. The line profile and average radial velocity curve constructed from its measurements carry information not about the orbital motion of the disk, but about the velocity field in an extended gas shell that is periodically perturbed by

the binary system immersed in it. The multicomponent structure of the profile, resolved at higher resolution, suggests that the variability of V_r can arise not only as a result of the orbital Doppler shift of the components but also due to changes in their relative intensities leading to the line profile asymmetry and formal shift of the effective line center. However, most flux from these line components is not eclipsed.

4.3. Orbital variability of the absolute He II emission flux

Due to light slit losses, the observed line fluxes can be underestimated by a factor weakly dependent on the wavelength. We can estimate this factor from broadband photometry by comparing the observed fluxes in some filter with those calculated from the spectra by integrating them with the filter transmission curve and detector sensitivity curve. More than half of our spectra are accompanied by photometric measurements taken within ± 5 hr that allow us to renormalize them. Based on these data, we constructed the dependence of the absolute line flux on the orbital phase and found that the flux varies almost sinusoidally with a semiamplitude of 0.2 mag: the line turns out to be the brightest at the phase $\varphi_{\text{orb}} = 0.5$, when the disk is in front of the donor star (Figure 4e). This variability cannot be caused by screening of a substantial part of the line forming region inside the binary system, because in this case the flux is expected to drop somewhere within the phases $\varphi_{\text{orb}} = 0.75 - 0.25$ and a plateau outside this range should appear, which is inconsistent with the observed sinelike flux variability in Figure 4e. Taking into account this variability and assuming that there are no eclipses of the He II 4686 Å line formation region, we superimposed the expected change in the equivalent width on its measurements and also obtained excellent agreement (cf. Figure 4d).

Note that the sinelike change in the He II 4686 Å line flux can be traced at different precessional phases, but at $\varphi_{\text{prec}} = 0$ the average flux is by $\approx 10\%$ higher than at the crossover phases and by $\approx 15\%$ higher than at $\varphi_{\text{prec}} = 0.5$. A similar variability, but with a larger amplitude of $\sim 100\%$, was observed in the H α emission line ([A. M. Cherepashchuk et al. 2022](#)).

5. CONCLUSION

Using the results of 6 yr of spectral and photometric monitoring of SS433 in 2020 – 2025 at CMO SAI MSU, we have found that the formation region of the He II 4686 Å emission line can experience only weak eclipses suggesting that the line formation region is significantly larger than the donor star size. The absolute flux in

the line against the randomly fluctuating background demonstrates a regular sinelike variability with the orbital period of SS433 and maximum around phase 0.5 (Figure 4e). The double-peaked profiles of the He II emission line and the nature of their variability are similar to those in the hydrogen and neutral helium emission lines, which were described by [M. G. Bowler \(2011\)](#) in the model of a rotating circumbinary envelope with azimuthal inhomogeneity. Such an inhomogeneity should naturally occur in the form of a spiral shock wave in the circumbinary gas due to the orbital motion of the components.

Our findings imply that it is incorrect to consider the radial velocity of the He II 4686 Å line as the radial velocity of the compact object, and therefore, the mass function estimates from the previous high-quality He II 4686 Å line measurements may not correspond to real values. The observed He II 4686 Å radial velocity curve (Figure 4a) cannot be used to reliably estimate the masses of the binary components in SS433.

ACKNOWLEDGEMENTS

The authors acknowledge the anonymous referee for useful comments. We thank the staff of the CMO SAI MSU for their help with observations. The study was conducted under the state assignment of M. V. Lomonosov Moscow State University. Scientific equipment used in this study was purchased partially through the M. V. Lomonosov Moscow State University Program of Development.

DATA AVAILABILITY

All observational data (spectra, B-photometry, and parameters of the He II line shown in Figures 2 and 4) are available at [doi:10.5281/zenodo.18311703](https://doi.org/10.5281/zenodo.18311703).

AUTHOR CONTRIBUTIONS

All authors contributed equally.

Facilities: SAI-2.5m, VLT:Kueyen

Software: astropy ([Astropy Collaboration et al. 2013, 2018, 2022](#)),

REFERENCES

Astropy Collaboration, Robitaille, T. P., Tollerud, E. J., et al. 2013, *A&A*, 558, A33, doi: [10.1051/0004-6361/201322068](https://doi.org/10.1051/0004-6361/201322068)

Astropy Collaboration, Price-Whelan, A. M., Sipőcz, B. M., et al. 2018, *AJ*, 156, 123, doi: [10.3847/1538-3881/aabc4f](https://doi.org/10.3847/1538-3881/aabc4f)

Astropy Collaboration, Price-Whelan, A. M., Lim, P. L., et al. 2022, *ApJ*, 935, 167, doi: [10.3847/1538-4357/ac7c74](https://doi.org/10.3847/1538-4357/ac7c74)

Berdnikov, L. N., Belinskii, A. A., Shatskii, N. I., et al. 2020, *Astronomy Reports*, 64, 310, doi: [10.1134/S1063772920040010](https://doi.org/10.1134/S1063772920040010)

Bowler, M. G. 2011, *A&A*, 531, A107, doi: [10.1051/0004-6361/201016381](https://doi.org/10.1051/0004-6361/201016381)

Cherepashchuk, A., Belinski, A., Dodin, A., & Postnov, K. 2023, *NewA*, 103, 102060, doi: [10.1016/j.newast.2023.102060](https://doi.org/10.1016/j.newast.2023.102060)

Cherepashchuk, A., Postnov, K., Molkov, S., Antokhina, E., & Belinski, A. 2020, *NewAR*, 89, 101542, doi: [10.1016/j.newar.2020.101542](https://doi.org/10.1016/j.newar.2020.101542)

Cherepashchuk, A. M. 1981, *MNRAS*, 194, 761, doi: [10.1093/mnras/194.3.761](https://doi.org/10.1093/mnras/194.3.761)

Cherepashchuk, A. M., Belinski, A. A., Dodin, A. V., & Postnov, K. A. 2021, *MNRAS*, 507, L19, doi: [10.1093/mnrasl/slab083](https://doi.org/10.1093/mnrasl/slab083)

Cherepashchuk, A. M., Dodin, A. V., & Postnov, K. A. 2025, arXiv e-prints, arXiv:2506.01106, doi: [10.48550/arXiv.2506.01106](https://doi.org/10.48550/arXiv.2506.01106)

Cherepashchuk, A. M., Dodin, A. V., Postnov, K. A., et al. 2022, *Astronomy Reports*, 66, 451, doi: [10.1134/S1063772922060026](https://doi.org/10.1134/S1063772922060026)

Crampton, D., Cowley, A. P., & Hutchings, J. B. 1980, *ApJL*, 235, L131, doi: [10.1086/183176](https://doi.org/10.1086/183176)

Crampton, D., & Hutchings, J. B. 1981, *ApJ*, 251, 604, doi: [10.1086/159505](https://doi.org/10.1086/159505)

D'Odorico, S., Oosterloo, T., Zwitter, T., & Calvani, M. 1991, *Nature*, 353, 329, doi: [10.1038/353329a0](https://doi.org/10.1038/353329a0)

Fabrika, S. 2004, *Astrophys. Space Phys. Res.*, 12, 1, doi: [10.48550/arXiv.astro-ph/0603390](https://doi.org/10.48550/arXiv.astro-ph/0603390)

Fabrika, S. N., & Bychkova, L. V. 1990, *A&A*, 240, L5

Filippenko, A. V., Romani, R. W., Sargent, W. L. W., & Blandford, R. D. 1988, *AJ*, 96, 242, doi: [10.1086/114806](https://doi.org/10.1086/114806)

Goranskij, V. 2011, *Peremennye Zvezdy*, 31, 5, doi: [10.48550/arXiv.1110.5304](https://doi.org/10.48550/arXiv.1110.5304)

Hillwig, T. C., Gies, D. R., Huang, W., et al. 2004, *ApJ*, 615, 422, doi: [10.1086/423927](https://doi.org/10.1086/423927)

Kubota, K., Ueda, Y., Fabrika, S., et al. 2010, *ApJ*, 709, 1374, doi: [10.1088/0004-637X/709/2/1374](https://doi.org/10.1088/0004-637X/709/2/1374)

Lu, W., Fuller, J., Quataert, E., & Bonnerot, C. 2023, *MNRAS*, 519, 1409, doi: [10.1093/mnras/stac3621](https://doi.org/10.1093/mnras/stac3621)

Margon, B. 1984, *ARA&A*, 22, 507, doi: [10.1146/annurev.aa.22.090184.002451](https://doi.org/10.1146/annurev.aa.22.090184.002451)

Picchi, P., Shore, S. N., Harvey, E. J., & Berdyugin, A. 2020, *A&A*, 640, A96, doi: [10.1051/0004-6361/202037960](https://doi.org/10.1051/0004-6361/202037960)

Potanin, S. A., Belinski, A. A., Dodin, A. V., et al. 2020,
Astronomy Letters, 46, 836,
doi: [10.1134/S1063773720120038](https://doi.org/10.1134/S1063773720120038)

Vernet, J., Dekker, H., D'Odorico, S., et al. 2011, A&A,
536, A105, doi: [10.1051/0004-6361/201117752](https://doi.org/10.1051/0004-6361/201117752)
Waisberg, I., Dexter, J., Petrucci, P.-O., Dubus, G., &
Perraut, K. 2019, A&A, 623, A47,
doi: [10.1051/0004-6361/201834746](https://doi.org/10.1051/0004-6361/201834746)